Scripta Materialia 189 (2020) 122–128

Contents lists available at ScienceDirect

Scripta Materialia

journal homepage: www.elsevier.com/locate/scriptamat

A novel test technique for the mechanistic study of initiation of environmentally assisted cracking on a Ni–30Cr–10Fe alloy in simulated pressurized water reactor primary water

Wenjun Kuang*, Han Yue, Xingyu Feng, Bo Yang, Chaowei Guo

Center for Advancing Materials Performance from the Nanoscale (CAMP-Nano), State Key Laboratory for Mechanical Behavior of Materials, Xi'an Jiaotong University, Xi'an 710049, PR China

ARTICLE INFO

Article history:
Received 22 July 2020
Revised 10 August 2020
Accepted 10 August 2020
Available online 21 August 2020

Keywords:
Nickel alloys
Scanning/transmission electron microscopy (STEM)
Diffusion-induced grain boundary motion (DIGM)
Stress corrosion cracking

ABSTRACT

Recurring step straining was developed to investigate the environmentally assisted cracking (EAC) initiation of a Ni-30Cr-10Fe alloy (Alloy 690) in simulated pressurized water reactor (PWR) primary water. Thanks to this technique, the roles of corrosion and straining in the EAC initiation of Alloy 690 was decoupled and typical microstructures in stress corrosion cracking, i.e. diffusion induced grain boundary migration and oxidation into the migration zone, were reproduced. Digital image correlation using indigenous surface oxide particles as markers was successfully incorporated into this technique for high-resolution in-plane strain measurement. The preliminary results show that intergranular crack initiation is correlated with the high local strain in both adjacent grains, indicating that slip transfer across the grain boundary promotes crack initiation. Recurring step straining is desirable for the mechanistic study of EAC as it makes the separate roles of chemical and mechanical processes adjustable and traceable.

Nickel base Alloy 690 is an important structural material in pressurized water reactors (PWRs). This material shows significantly higher stress corrosion cracking (SCC) resistance than its predecessor-Alloy 600 in the primary water environment [1–4]. The high resistance to SCC in Alloy 690 is reflected by the difficulty to initiate cracking in this alloy in simulated PWR primary water with conventional constant deflection or constant load techniques [5]. Now increasing evidence shows that the high resistance to SCC initiation of Alloy 690 is related to the formation of a compact oxide film over the random high angle boundary (RHAB) [6–8] which suppresses the penetrative intergranular oxidation. Nonetheless, SCC of Alloy 690 can be consistently initiated by dynamic straining [5,9–11] and an initiation model was proposed by Moss et al. [5]. Recently, Kuang and Was [12] characterized the microstructures of grain boundaries at different SCC initiation stages after constant extension rate tensile (CERT) test to further substantiate the model. The microstructure analysis of SCC cracks formed on Alloy 690 [13] also suggests that diffusion induced grain boundary migration (DIGM) and penetrative oxidation into the migration zone are two important precursors in the SCC process.

Although significant progress has been made in the SCC study of Alloy 690 in simulated PWR primary water, there are still some unresolved issues. On the one hand, it is difficult to reveal the full process of SCC initiation through post-test analysis. SCC is a complicated process which involves the coupling of environmental degradation and mechanical deformation. The previous work normally characterizes the sample after SCC test is finished. It only captures a static frame of the whole SCC process and the separate roles of corrosion and deformation cannot be clearly identified. Ex-situ straining after exposure test has been used to single out the mechanical process in the initiation of environmentally assisted cracking (EAC) of alloy 600 [14–17]. Unfortunately, such one step straining couldn't initiate cracking on Alloy 690 [18]. On the other hand, the previous work indicates that dynamic straining is crucial in driving the SCC initiation on Alloy 690 [5,10]. However, the mechanism of straining effect in SCC initiation is still not clear. Addressing this issue necessitates the measurement of local strain distribution near a grain boundary during plastic deformation. Digital image correlation (DIC) has been widely used for local strain measurement [19]. To apply DIC for SCC initiation study in high temperature water, the DIC markers should be compatible with the harsh environment. Noble metal grid has been used for this purpose [20]. Nevertheless, in addition to causing possible interference on the corrosion process, depositing a thin layer of noble metal is complicated and only covers a small area of interest. Marrow et al.

* Corresponding author.
E-mail addresses: wjkuang66@xjtu.edu.cn, wjkuang66@gmail.com (W. Kuang).

https://doi.org/10.1016/j.scriptamat.2020.08.016
1359-6462/

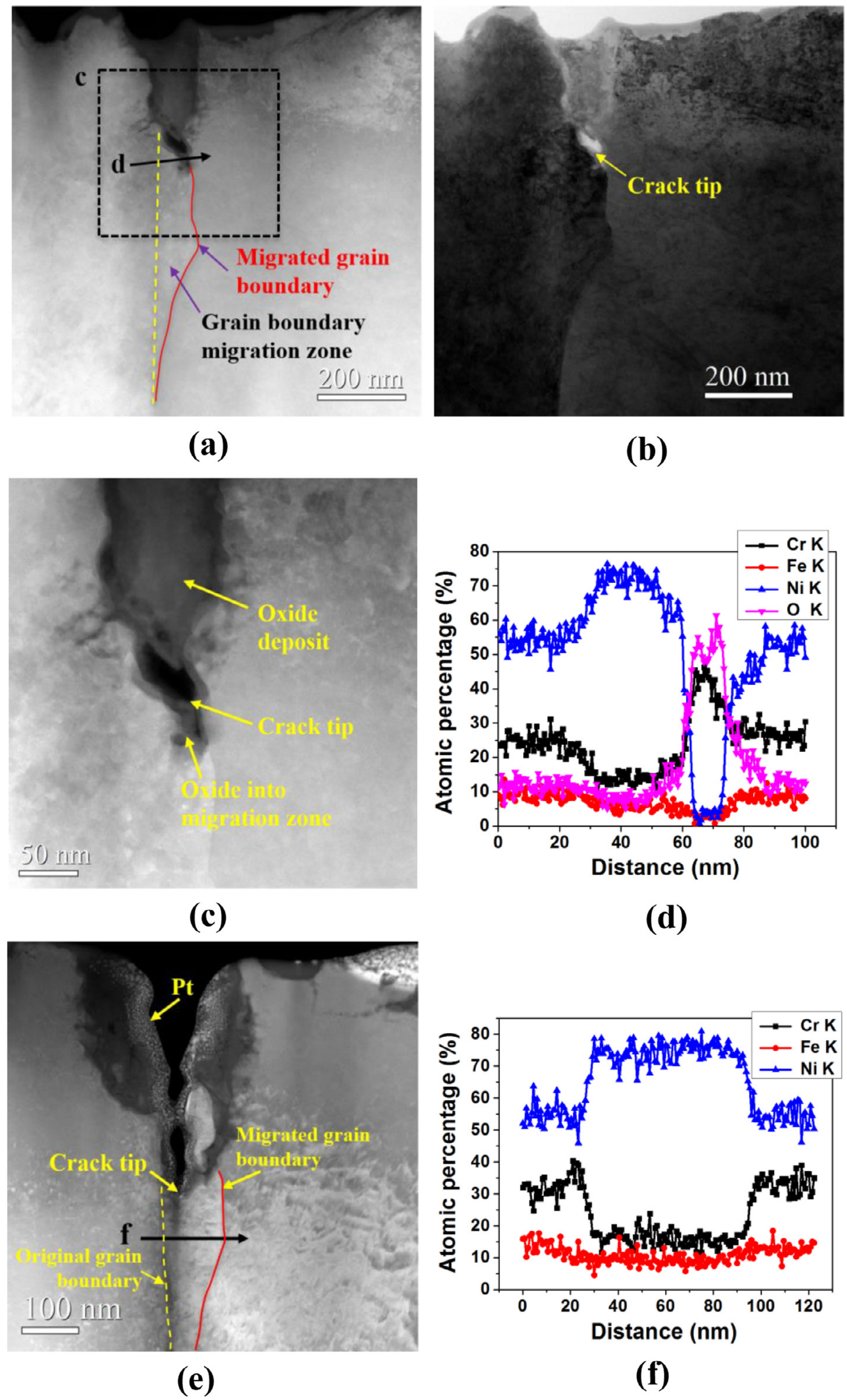

Fig. 1. (a) High angle annular dark-field (HAADF) and (b) bright field images of grain boundary A after 4th exposure, (c) enlarged HAADF image from framed area in (a), (d) energy dispersive spectroscopy (EDS) line profile across the line in (a), (e) HAADF image of grain boundary A after 4th straining and (f) EDS line profile across the line in (e).

[21,22] produced DIC markers on stainless steel by electro-etching and studied the cracking processes in high temperature water by taking optical images through a windowed autoclave. In this technique, the electro-etching would inevitably affect the cracking behavior of material and the produced DIC marker maybe covered by the oxide particles formed by precipitation during exposure to high temperature water. Moreover, the optical system only covers a fixed area of interest at limited resolution. Therefore, the test technique needs to be further improved to advance the mechanistic understanding of SCC initiation on Alloy 690.

In this work, recurring step straining was developed to investigate the EAC initiation of Alloy 690 in 350 °C simulated PWR primary water. The chemical composition of Alloy 690 used in this work is 59.3 wt% Ni, 29.4% Cr, 10.2% Fe, 0.31% Mn, 0.14% Al,

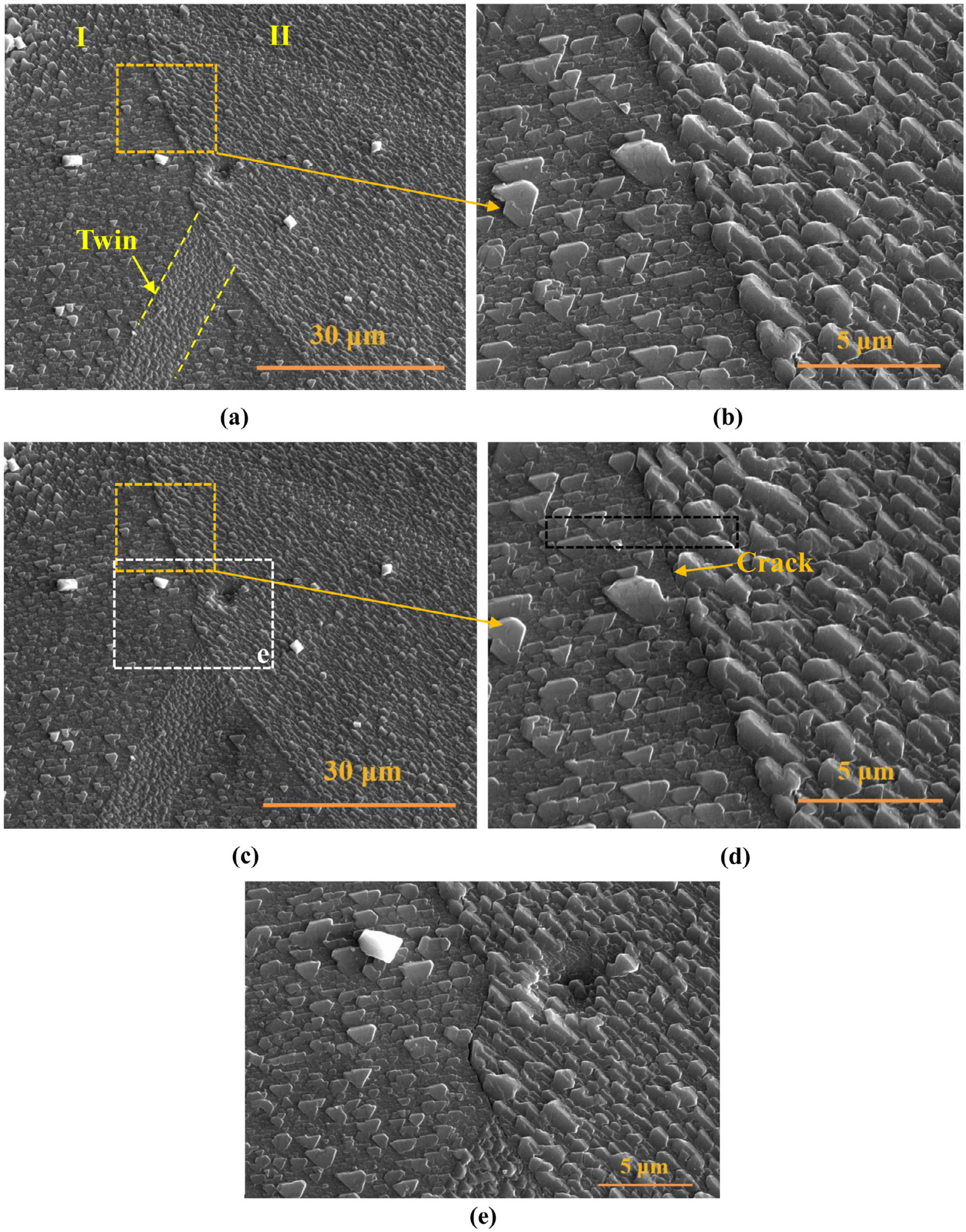

Fig. 2. (a) and (b) SEM images of sampled grain boundary B after 4th exposure, (c) and (d) SEM images of sampled grain boundary B after 4th straining, (e) enlarged image from frame e in (c). The black dashed frame in (d) marks the position for FIB cutting.

0.25% Si and 0.02% C. The bulk material was solution annealed (SA) at 1100 °C for 1 h and water quenched. Round tensile bars with 20 mm in gauge length and 2 mm in diameter were machined from the bulk material. As in our previous work [9,23], the gauge section of the tensile bar was mechanically abraded up to 4000 grit and electropolished for 30 s at 30 V in a solution of 10% (volume fraction) perchloric acid in methanol which was cooled to −30 °C. All the samples were cleaned three times alternately with methanol and acetone immediately after electropolishing.

The tensile bar was exposed in a refreshed stainless steel autoclave without being loaded. The environment was 350 °C water with 2 ppm Li (as LiOH), 1000 ppm B (as H_3BO_3). The dissolved hydrogen concentration was maintained at 19.7 cm^3 (STP) H_2/kg H_2O. After the exposure, the sample was taken out and examined in a FEI Helios SEM with the tensile axis aligned with the horizon-

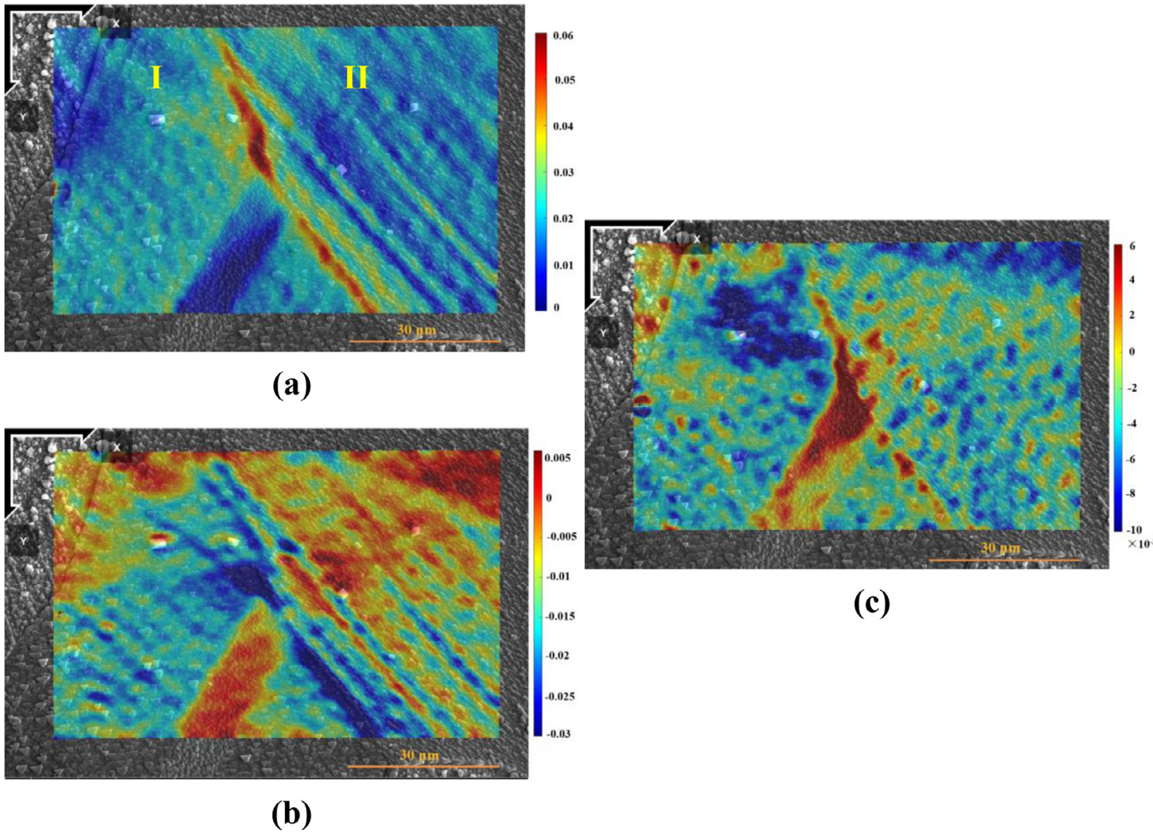

Fig. 3. Measured strain (a) *XX*, (b) *YY* and (c) *XY* from grain boundary B after 4th straining by digital image correlation (DIC). Tensile direction was along the *X* axis.

Table 1
Details of the experiment steps.

	1st step	2nd step	3rd step	4th step
Exposure time (h)	648	140	255	1031
Plastic strain	2.4%	1.9%	1.9%	2.0%
Final stress (MPa)	284	292	337	364

tal direction. Secondary electron (SE) imaging mode was used. The acceleration voltage was 30 kV and beam current was set to 1.6 nA. Around 20 grain boundaries were examined, and the positions of those boundaries were recorded. Then the sample, which has a yield strength of 255 MPa and a uniform elongation of 53.5%, was strained ~2% on an MTS machine at 0.15 mm/min in air at room temperature. Afterwards, the sample was put back into the SEM and the previous grain boundaries were tracked and reexamined to see if the straining induced crack initiation. These steps were repeated several times. The exposure time, applied plastic strain and the final stress for each step are listed in Table 1. The SEM images taken before and after the step straining were used for DIC analysis with the indigenous surface oxide particles serving as DIC markers. An open-source 2D DIC software (Ncorr) was used to process the images [24]. The resolution of strain measurement is around 10^{-4} with the algorithm used in the software [25]. To get a good trade-off between resolution and noise, the subset radius, subset spacing, strain radius, were set as 15, 1, 10 pixels. The spatial resolution is around 0.24 μm based on the SEM imaging condition. Cross sections of some grain boundaries were cut using focused ion beam (FIB) milling on a FEI Helios Nanolab per the procedure used before [8,12,13]. The element composition and microstructure were analyzed with scanning transmission electron microscope (STEM) JEOL 2100 which is equipped with an Octane Super silicon drift energy dispersive spectroscopy (EDS) X-ray detector system, a bright field detector and a high angle annular dark-field (HAADF) detector. Some EDS line profiles were also acquired in a JEOL JEM-F200(HR) microscope which is equipped with two 100 mm^2 EDS X-ray detectors.

Grain boundary A was sampled as it shows crack initiation after 3rd straining. Fig. 1(a) and (b) are HAADF and bright field images of the cross section of grain boundary A after 4th exposure. The crack is filled with oxide which formed by precipitation because the stainless-steel autoclave would generate a local high concentration of Fe ion which deposits onto the sample surface as spinel particles [26,27]. There is a grain boundary migration zone beyond the oxide with a curly migrated grain boundary on the right. DIGM has long been reported in this alloy [6,7,13,28] when exposed to high temperature reducing water or steam. The bright field image shows that the area near the oxide tip is as bright as the open space above the sample (Fig. 1(b)), confirming that this area corresponds to an open crack. The trace of migrated grain boundary is readily identified from Fig. 1(b) as the two grains show different contrasts. Fig. 1(c) is an enlarged image from the dashed frame in Fig. 1(a). The open crack beyond the oxide deposit appears darker on the HAADF image and the forefront point corresponds to the crack tip (Fig. 1(c)). Beyond the crack tip, it is found that oxide forms along the migrated grain boundary and extends into the migration zone, consistent with a previous work [13]. Fig. 1(d) shows the EDS profile along line d in Fig. 1(a). The migration zone is enriched in Ni and depleted in Cr while the oxide shows significant Cr enrichment (Fig. 1(d)). The intergranular oxide beyond SCC crack has been revealed to be composed of NiO and Cr_2O_3 [13]. After 4th straining test, another FIB sample was made from grain boundary A. Fig. 1(e) shows the HAADF image of the cross section. The crack can only extend as far as the intergranular oxidation advances, consistent with the results from miniature cantilever bend test on oxidized grain boundary of alloy 600 [15]. Therefore, the

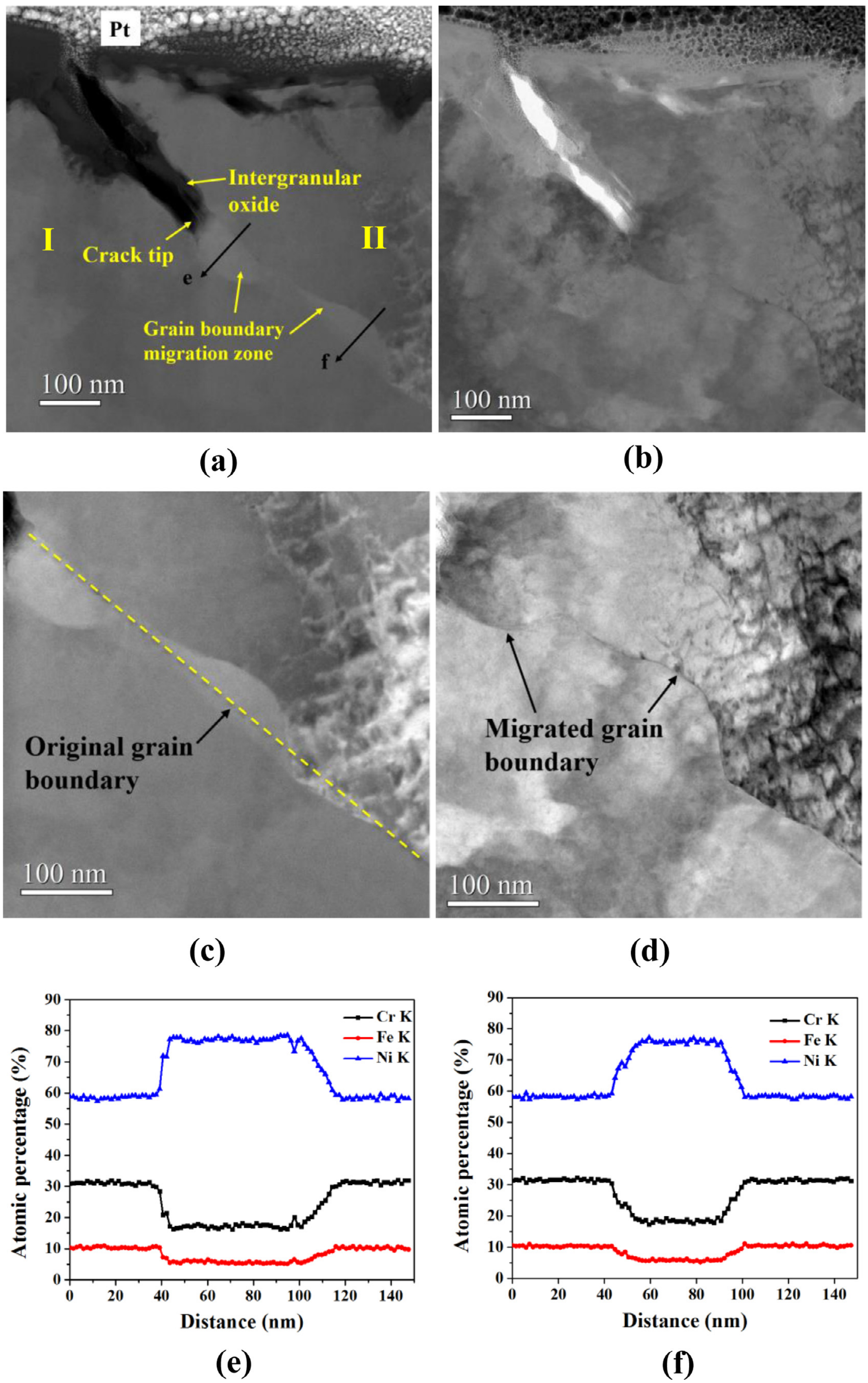

Fig. 4. (a) HAADF and (b) bright field images of the grain boundary cross section cut from Fig. 2(d), (c) HAADF and (d) bright field images of grain boundary migration zone beyond the crack tip, (e) and (f) EDS line profiles across the lines in (a).

intergranular oxidation is an inevitable precursor for SCC cracks to initiate or propagate. The EDS line profile along line f in Fig. 1(e) consistently shows that the migration zone is enriched in Ni and depleted in Cr (Fig. 1(f)).

A previous foil-fracture test [18] indicated that one step straining after exposure test could not induce intergranular cracking on Alloy 690. That is mainly due to its ability to form a protective oxide film over RHAB [6–8,28] which suppresses the penetrative intergranular oxidation. Here it is demonstrated that recurring step straining can induce crack initiation on this alloy. The protective oxide film over grain boundary A should have been breached during the previous straining and penetrative oxidation ensued thereafter. The oxide film over the grain boundary was not repaired during exposure even when no stress or strain was applied. Therefore, the breach of surface oxide film over RHAB, which is a crucial precursor to crack initiation on Alloy 690, can also be caused by step straining as in this work.

Crack initiation was captured on grain boundary B right after 4th straining. Fig. 2(a) and (b) shows the SEM images of grain boundary B after 4th exposure. A twin in the left grain (grain I) intersects the grain boundary (Fig. 2(a)). No crack is observed on the enlarged image in Fig. 2(b). Interestingly, after 4th straining test, the enlarged SEM image shows intergranular crack initiation (Fig. 2d)). The enlarged image from frame e in Fig. 2(c) shows that the crack was terminated by the twin intersection (Fig. 2(e)). DIC analysis from the SEM images taken before and after 4th straining was conducted. The strain distribution near this grain boundary is shown in Fig. 3. The tensile direction was aligned with the X axis. Fig. 3(a) clearly shows that the XX strain along the grain boundary reaches local maximum except the section where the twin emerges. That is because the crack initiation creates opening along the grain boundary which is treated as displacement in DIC software. The XX strain along the grain boundary decreases rapidly where the twin intersects the right grain (grain II), confirming that crack initiation was suppressed by the twin. It is interesting to find that grain I shows a relatively uniform XX strain near 2% while the strain in the twin is almost 0% (Fig. 3(a)). It is worth mention that the upper part of the twin close to the cracked grain boundary shows local distribution of relatively small strain (Fig. 3(a)), which should result from the concentrated stress state near the crack tip. Consistently, the YY strain in grain I is mostly negative while that in most of the twin is still around 0% (Fig. 3(b)). Fig. 3(c) shows the distribution of XY strain. The maximum value (around 0.6%) lies in the crack and extends to the twin interior. From Fig. 3, the higher susceptibility to crack initiation of grain boundary is well correlated with the higher plastic strain in the adjacent grains. It suggests that high local strain in both grains, i.e. easy slip transfer across the grain boundary, promotes the crack initiation of grain boundary. In contrast, according to the local stress analysis by McMurtrey et al. [29] and Jonson et al. [30], when the dislocation channel transfer was impeded at a grain boundary, the dislocation pile-up would raise the local stress and increase the susceptibility to SCC initiation on ion-irradiated stainless steel. Therefore, local strain is probably the controlling factor in the fracture of surface oxide film over RHAB and hence the SCC initiation for alloy 690.

A cross section was sampled from the black frame in Fig. 2(d). Fig. 4(a) and (b) shows the HAADF and bright field images of the cross section. The crack has a mixed route. It starts from the oxide/grain II interface, goes through the intergranular oxide and extends along the grain I/oxide interface. The crack reaches the end of the intergranular oxide as in Fig. 1(e). The exposed grain matrixes along the crack flanks are almost free of oxidation, confirming that this crack was freshly generated during 4th straining. The HAADF and bright field images of migration zone beyond the crack are shown in Fig. 4(c) and (d). The original grain boundary is represented by a yellow broken line (Fig. 4(c)) and the migrated boundary can be readily identified in the bright field image (Fig. 4(d)). Apparently, this grain boundary migrated in both directions. The EDS profiles along the lines in Fig. 4(a) confirm that the migration zone is enriched in Ni and depleted in Cr (Fig. 4(e) and (f)).

In this study, the main process of crack initiation, i.e. the intergranular oxidation along the DIGM zone and fracture of the oxide or the oxide/matrix interface is clearly revealed. The evidence shown here supports the SCC initiation model proposed by Moss et al. [5] and agrees with the previous characterization results [12,13]. Thus, recurring step straining can be a valid technique for the mechanistic study of the SCC initiation behavior of Alloy 690. Some limitations should be noted for this new technique. The effect of mechanical loading on the corrosion process could not be simulated in the recurring step straining test as the sample is not loaded during corrosion. It is also not meaningful to quantitatively compare the cracking result from recurring step straining test with that from CERT test. That is because both techniques accelerate the process of crack initiation, but to different degrees due to the difference in straining condition.

Compared with CERT, recurring step straining does have some attractive advantages. Firstly, it decouples the effects of corrosion and straining and the separate roles of chemical and mechanical processes in SCC can closely traced. Prior to step straining, the corrosion process is paused by taking the sample out of harsh environment and the corrosion-induced microstructure changes can be thoroughly investigated. Thus, how corrosion contributes to crack initiation can be revealed. More importantly, the ex-situ step straining can be well controlled, and the resultant local strain state and mechanical response of microstructures can be examined in detail. Secondly, the decoupling of corrosion and straining allows the local strain distribution to be measured at high resolution without introducing extraneous DIC markers (Fig. 3). The current DIC technique is ideal for the EAC initiation study as it uses indigenous oxide particles as markers without causing extra interference and the resolution is high enough to capture the local strain distribution. Therefore, recurring step straining is a quasi in-situ test technique which allows a thorough investigation on the full process of cracking. It is a desirable alternative to CERT when studying SCC in harsh environment like high temperature high pressure water which precludes the use of in-situ test technique. Lastly, the severities of corrosion and mechanical straining can be readily adjusted by changing the length of corrosion time and the applied strain to match the properties of tested material. While in a CERT test, strain rate is used to balance the severity of corrosion with mechanical straining [9]. A very low strain rate ($\sim 10^{-8}$/s) is normally needed to initiate SCC on resistant material like Alloy 690 which is very challenging to acquire.

Data availability

The raw/processed data required to reproduce these findings cannot be shared at this time as the data also forms part of an ongoing study.

Declaration of Competing Interest

There is no conflict of interest.

Acknowledgments

The authors acknowledge the financial support of National Natural Science Foundation of China (No. 51971172) and the Young Talent Support Plan of Xi'an Jiaotong University.

References

[1] K. Smith, A. Klein, P. Saint-Paul, J. Blanchet, in: Proceedings of Second International Symposium on Environmental Degradation of Materials in Nuclear Power Systems-Water Reactors, American Nuclear Society, Monterey, California, 1985.
[2] T. Yonezawa, K. Onimura, N. Sasaguri, T. Kusakabe, H. Nagano, K. Yamanaka, T. Minami, M. Inoue, in: Proceedings of Second International Symposium on Environmental Degradation of Materials in Nuclear Power Systems-Water Reactors, American Nuclear Society, Monterey, California, 1985.
[3] K. Norring, J. Engstrom, P. Norberg, in: Proceedings of Third International Symposium on Environmental Degradation of Materials in Nuclear Power Systems — Water Reactors, Traverse city, Michigan, 1987.
[4] T. Maeguchi, K. Sakima, K. Sato, K. Fujimoto, Y. Nagoshi, K. Tsutsumi, in: Proceedings of Eighteenth International Conference on Environmental Degradation of Materials in Nuclear Power Systems-Water Reactors, Portland, OR, USA, 2017.
[5] T. Moss, W. Kuang, G.S. Was, Curr. Opin. Solid State Mater. Sci 22 (2018) 16–25.
[6] M.J. Olszta, D.K. Schreiber, M.B. Toloczko, S.M. Bruemmer, in: Proceedings of Sixteenth International Conference on Environmental Degradation of Materials in Nuclear Power Systems-Water Reactors, Asheville, North Carolina, USA, 2013.
[7] T. Moss, G. Cao, G.S. Was, Metall. Mater. Trans. A (2017) 1–17.
[8] W. Kuang, G.S. Was, Acta Mater. 182 (2020) 120–130.
[9] W. Kuang, G.S. Was, Corros. Sci. 97 (2015) 107–114.
[10] P.L. Andresen, M. Morra, K. Ahluwalia, in: Proceedings of Conference on Contribution of Materials Investigations and Operating Experience to LWRs' Safety, Performance and Reliability, France, 2015.
[11] W. Kuang, G.S. Was, C. Miller, M. Kaufman, T. Alam, B. Gwalani, R. Banerjee, Corros. Sci. 130 (2018) 126–137.
[12] W. Kuang, G.S. Was, Corros. Sci. 163 (2020) 108243.
[13] W. Kuang, M. Song, G.S. Was, Acta Mater. 151 (2018) 321–333.
[14] K. Fujii, T. Miura, H. Nishioka, K. Fukuya, in: Proceedings of Fifteenth International Conference on Environmental Degradation of Materials in Nuclear Power Systems-Water Reactors, Colorado Springs, Colorado, USA, 2011.
[15] H. Dugdale, D.E.J. Armstrong, E. Tarleton, S.G. Roberts, S. Lozano-Perez, Acta Mater. 61 (2013) 4707–4713.
[16] A. Stratulat, D.E.J. Armstrong, S.G. Roberts, Corros. Sci. 104 (2016) 9–16.
[17] T. Couvant, J. Caballero, C. Duhamel, J. Crépin, T. Maeguchi, in: Proceedings of the Eighteenth International Conference on Environmental Degradation of Materials in Nuclear Power Systems – Water Reactors, Springer International Publishing, Cham, 2018.
[18] R.C. Newman, T.S. Gendron, P.M. Scott, in: Proceedings of the Ninth International Symposium on Environmental Degradation of Materials in Nuclear Power Systems- Water Reactors, Newport Beach, CA, USA, 1999.
[19] B. Pan, Measur. Sci. Technol. 29 (2018) 082001.
[20] T. Couvant, L. Legras, T. Ghys, P. Gambier, N. Huin, G. Ilevbare, in: Proceedings of the Fifteenth International Conference on Environmental Degradation of Materials in Nuclear Power Systems-water reactors, Colorado Springs, Colorado, USA, 2011.
[21] J.A. Duff, T.J. Marrow, Corros. Sci. 68 (2013) 34–43.
[22] A. Stratulat, J.A. Duff, T.J. Marrow, Corros. Sci. 85 (2014) 428–435.
[23] W. Kuang, G.S. Was, Scripta Mater. 107 (2015) 107–110.
[24] J. Blaber, B. Adair, A. Antoniou, Exp. Mech. 55 (2015) 1105–1122.
[25] B. Pan, H. Xie, Z. Guo, Hua T, Opt. Eng. 46 (2007) 033601.
[26] W. Kuang, X. Wu, E.-H. Han, J. Rao, Corros. Sci. 53 (2011) 3853–3860.
[27] W. Kuang, M. Song, P. Wang, G.S. Was, Corros. Sci. 126 (2017) 227–237.
[28] L. Volpe, M.G. Burke, F. Scenini, Corros. Sci. 167 (2020) 108514.
[29] M.D. McMurtrey, B. Cui, I. Robertson, D. Farkas, G.S. Was, Curr. Opin. Solid State Mater. Sci. 19 (2015) 305–314.
[30] D.C. Johnson, B. Kuhr, D. Farkas, G.S. Was, Acta Mater. 170 (2019) 166–175.